Fast model of a Hybrid Excitation Synchronous Machine using equivalent reluctance networks for parameter design

Quentin Loeuillet, Christian Chillet, Laurent Gerbaud, Jean-Claude Mipo, Jean-Luc Schanen

Fast model of a Hybrid Excitation Synchronous Machine using equivalent reluctance networks for parameter design

Quentin Loeuillet
Univ. Grenoble Alpes G2ELab
Grenoble, France
quentin.loeuillet@g2elab.grenoble-inp.fr

Christian Chillet
Univ. Grenoble Alpes G2ELab
Grenoble, France
christian.chillet@g2elab.grenoble-inp.fr

Laurent Gerbaud
Univ. Grenoble Alpes G2ELab
Grenoble, France
laurent.gerbaud@g2elab.grenoble-inp.fr

Jean-Claude Mipo
Valeo Electrical Systems
Créteil, France
jean-claude.mipo@valeo.com

Jean-Luc Schanen
Univ. Grenoble Alpes G2ELab
Grenoble, France
jean-luc.schanen@g2elab.grenoble-inp.fr

***Abstract*—The paper deals with a modeling approach for a hybrid excitation synchronous machine using equivalent reluctance networks. From a finite element modeling (used as a reference model), it aims to define a computationally efficient model suitable for integration with optimization algorithms. Therefore, it propose to perform a parameter design model of the electrical machine. One of the main ideas is to have a model enabling the machine design with or without permanent magnet. Firstly, the paper depicts the geometric parameterization of the machine. Then, it presents the development of a reluctance network model. This approach offers a compromise between accuracy and computational efficiency, making it suitable for future optimization tasks in the design and control of synchronous machines.**

Keywords—Double-excitation – Synchronous Motor – Reluctance Network – Optimization

I. INTRODUCTION

The design of synchronous machines demands models striking a compromise between computational efficiency and accuracy. While traditional finite element modeling (FEM) ensures accuracy, it often incurs significant computational time. Conversely, simpler experimental designs may lack the requisite accuracy for intricate optimization tasks. Bridging this gap, a reluctance-based modeling (RBM) approach emerges as a good compromise. Characterized by meticulous parameterization, this approach provides faster computation than FEM while maintaining good accuracy.

The large number of design parameters tends to favor gradient-based algorithms over stochastic algorithms. Gradient-based algorithms have demonstrated their effectiveness at finding innovative solutions within large and highly constrained solution spaces. Their convergence is however highly sensitive to the accuracy of the derivatives, what can be obtained directly with RBM. Therefore, to have a model that can be derivated in an exact way (eliminating the need for finite differences) is recommended with gradient-based optimization algorithm (suitable for some hundreds of sizing constraints).

Therefore, the paper focuses on such a parametrized model for the sizing of a hybrid excitation synchronous machine (HESM) [1-3]. However, challenges such as variable (non-uniform) air gap and trade-offs between wound and magnet excitation are the main originality of this paper, giving complementary element of analysis compared to [4].

In this way, the paper introduces the geometric parameterization of a double-excitation machine with tangential magnets. Then, a reluctance network modeling approach is presented, addressing the challenge of variable air gap modeling. Finally, the paper concludes by comparing the results obtained with the finite element method in terms of both accuracy and computational times.

II. PRESENTATION OF THE MOTOR TOPOLOGY

The studied motor topology is a parallel hybrid excitation synchronous motor [5] based on [6] (see Fig. 1.).

The topology combines the base structure of a wound rotor synchronous motor (WRSM) and incorporates additional interpolar magnets with tangential magnetization direction.

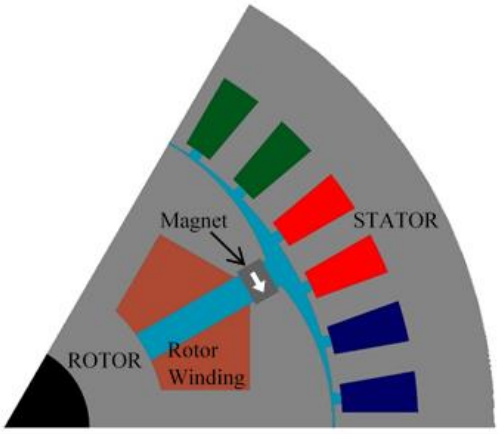

Fig. 1. Representation of 1/6th of the chosen HESM structure

Its stator has two slots per pole and per phase and is depicted here in a configuration with three pairs of poles, although the number of pole pairs can be adjusted as a sizing parameter. The model is fully parameterized, consisting of 20 independent geometric parameters. These geometric parameters are described along the paper when necessary.

Figure 2 gives a representation of a global flux mapping obtained by FEM, for the reference structure of the machine studied in the paper. It mainly illustrates the combination of the two excitations. The difficulty in the sizing of such an

electrical machine, is to have a good balance of the two excitations without having too much permanent magnets.

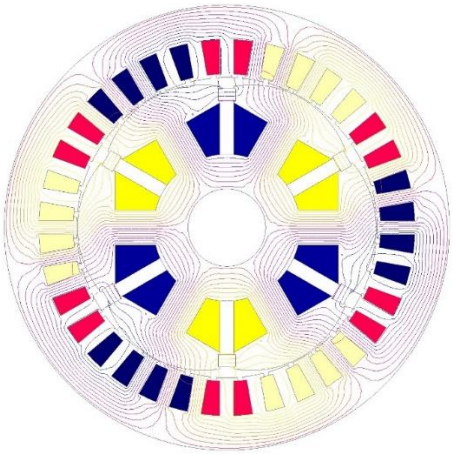

Fig. 2. Flux mapping of the motor obtained by FEM.

II. MODELING BY EQUIVALENT RELUCTANCE NETWORK

A. Modeling Approach

The modeling approach is based on the reluctance modeling theory [7]. It starts with the linear stator modeling, assuming a solid rotor with infinite permeability and a fixed air gap, following these steps:

- first, a single tooth is excited to identify stator iron reluctances and leakage reluctances.
- second, a three-phase source model is implemented to extend the validity to the entire stator.
- third, the magnetic non-linearity is integrated through the law described in equation (1), giving the induction B as a function of the magnetic field H,

$$B(H) = \mu_0 . H + J_S . \frac{Ha+1-\sqrt{(Ha+1)^2-4.Ha.(1-a)}}{2.(1-a)} \quad (1)$$

$$with \quad Ha = \mu_0 . H . \frac{\mu_r - 1}{J_S}$$

where μ_r is the relative permeability, J_S is the saturation magnetization, and a is a shape coefficient. A graphical interpretation of these coefficients is displayed in figure 3.

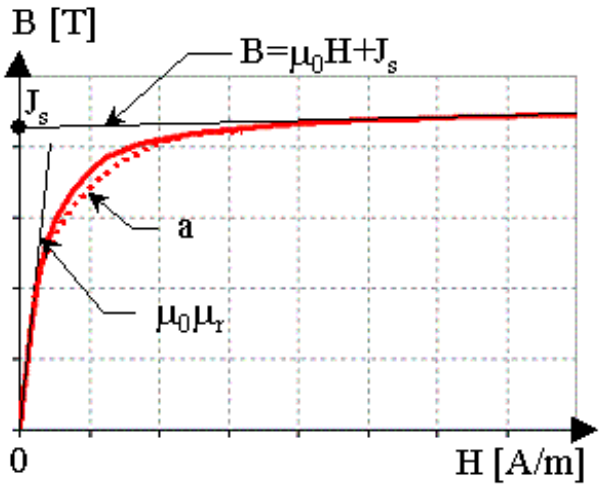

Fig. 3. Graphical interpretation of B(H) analytical law

This analytical expression is fitted from real material data using least square interpolation. The same analytical expression is used both for RBM and FEM computation, insuring no deviation during the validation process.

Then, the modeling of the air gap is considered, with the assumption of an infinitely permeable rotor:

- first, a parametrized model based on 3 reluctances by tooth, function of the air gap and slot opening value is proposed and validated
- to address variable air gap, a fixed air gap model validation is extended through discretization

Finally, the rotor model is integrated into the overall modeling framework, following the same approach than the stator one's.

This stepwise approach allows a comprehensive representation of the global motor electromagnetic behavior. It presents the complexities of the interaction between the stator, the air gap, and the rotor, while ensuring the incorporation of nonlinear effects at each stage of the process.

B. Modeling of the stator

1) Calculation of stator iron and leakage reluctances

To be able to isolate the magnetic behavior of a stator tooth, a FEM simulation with only one winded tooth is performed. Figure 4 shows the flux paths in the stator iron as wheel as leakage flux between teeth and between teeth isthmus.

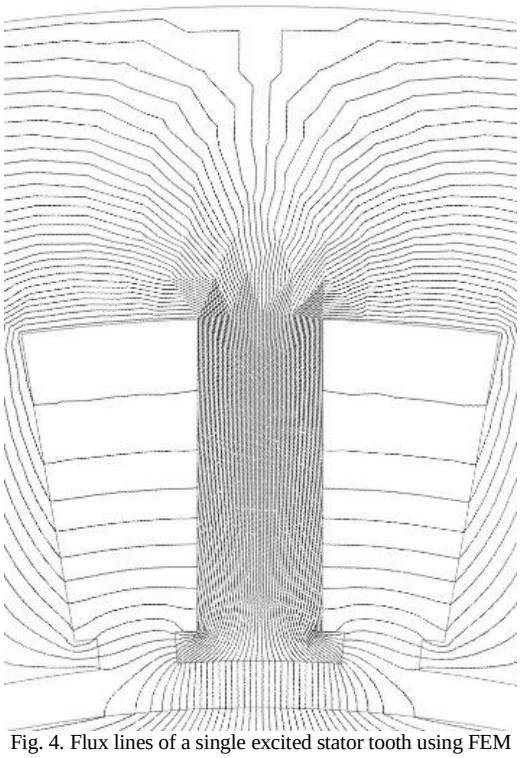

Fig. 4. Flux lines of a single excited stator tooth using FEM

Figure 5 shows the chosen discretization of the stator on a tooth pitch. The tooth reluctance is cut into two equal part, enabling the connection of the inter-teeth flux leakage reluctance.

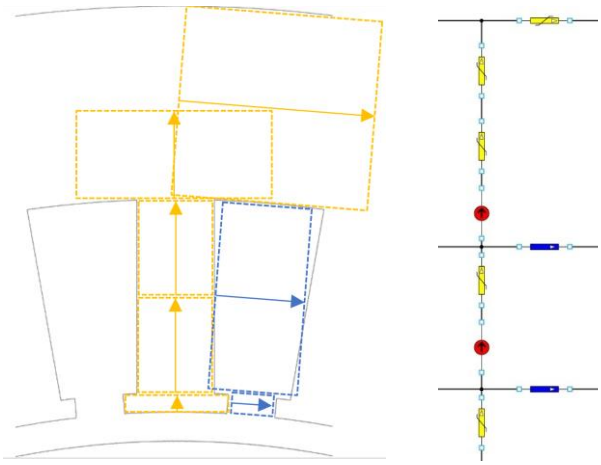

(a) (b)

Fig. 5. Identification of stator reluctances on one tooth pitch (a) schematics of the modeled reluctances (b) equivalent magnetic circuit

The calculation of iron related reluctances follows equation (2) using exact geometrical dimensions.

$$\Re = \frac{1}{\mu_0 \cdot \mu_r} \cdot \frac{l}{S} \qquad (2)$$

where μ_r is the iron relative magnetic permeability, l and S are respectively the length and the surface of the magnetic reluctance.

Concerning inter-teeth and slot opening flux leakage reluctance, a base value is defined using exact geometrical values. The length being identical, the surface is adjusted depending on air gap reluctances behavior with the values of air gap and slot opening. This aspect is discussed in section C. 1).

The tooth model of Fig. 5 (b) is then duplicated to obtain the full stator model. Figure 6 shows the resulting circuit for a 3-phase stator pole, using symmetries, for a configuration with two slots per pole and per phase.

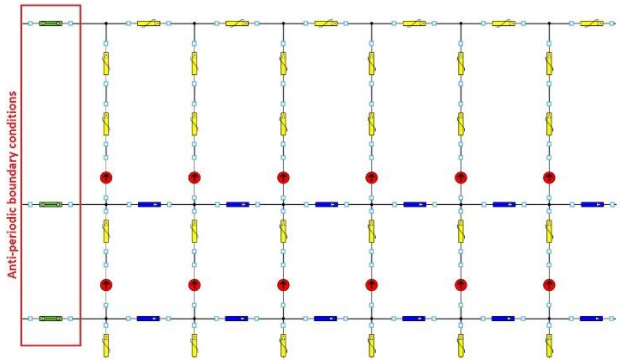

Fig. 6. Equivalent magnetic circuit of a 3-phase stator pole with two slots per pole and per phase

The use of anti-periodic boundary conditions enables a model using only the representation of a single pole of the motor (red part at the left in figure 6).
This contributes to reduce the size of the Jacobian matrix associated with the circuit as well as to reduce the computation times.

This type of modelling approach is particularly convenient for gradient-based optimization algorithm as the number of pairs of poles become a continuous variable, and thus can be used as an optimization variable. Paper [8] demonstrated the interest of such a relaxation of discrete formulations to improve optimization problem setting by optimizing an imaginary design space, i.e. with continuous variables instead of discrete variable even if the modelling is not realistic.

2) Calculation of equivalent current sources

Fig. 7. shows the equivalent current source values related to each tooth.

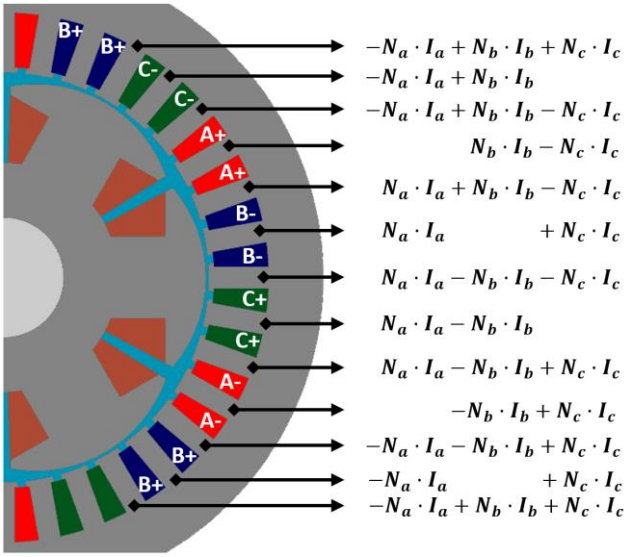

Fig. 7. 3-phase equivalent current sources by tooth

The current value is then divided by two to accommodate with the two source by tooth model presented in figure 5.(b).

C. Modeling of the Airgap

1) Pametric analysis : influence of the air gap and the slot opening on the air gap and leakage flux

In order to propose an acceptable model for the air gap, an extensive study of the flux path dependencies with geometrical parameters was conducted using FEM. The air gap and the slot opening values have been identified as the most influential parameters. Figure 8 presents the influence of these parameters on the flux paths.

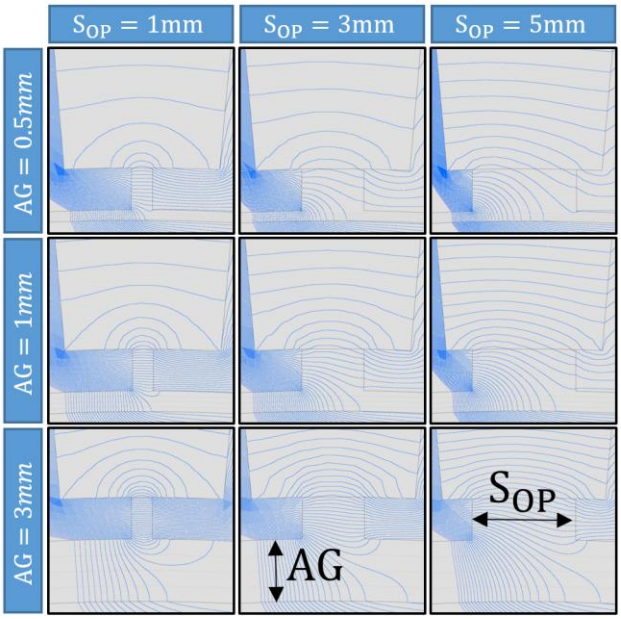

Fig. 8. FEM simulation zoomed on stator slot opening for different values of air gap AG and slot opening S_{OP}

To cover the largest parametric variation, the reluctance decomposition displayed in figure 9 is proposed.

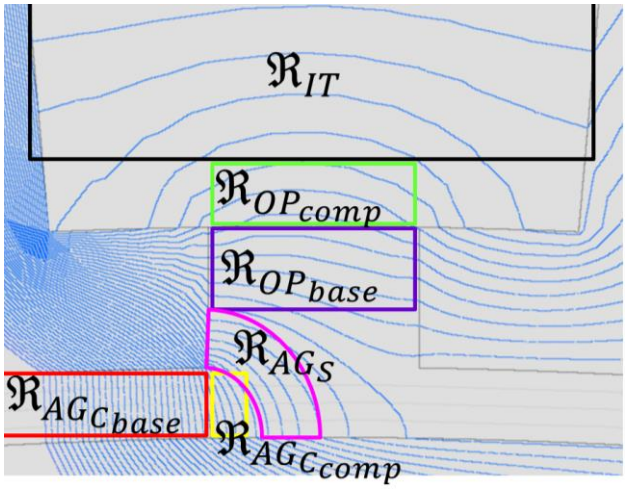

Fig. 9. Proposed flux decomposition of air gap and flux leakage reluctances

This decomposition exhibits base reluctances with formula strictly linked to geometrical parameters and complementary reluctances following linear expressions with air gap and slot opening values that enables the model to fit with FEM simulations.

First, in section C.2), the paper proposes to establish such a model in the case of fixed air gap value. Then, in section C.3), the model is extended to the case of a variable air gap value.

2) First approach on a fixed air gap

In the case of a fixed air gap, according to the observation of the flux in figure 10, the air gap model can be reduced to three reluctances by stator tooth.

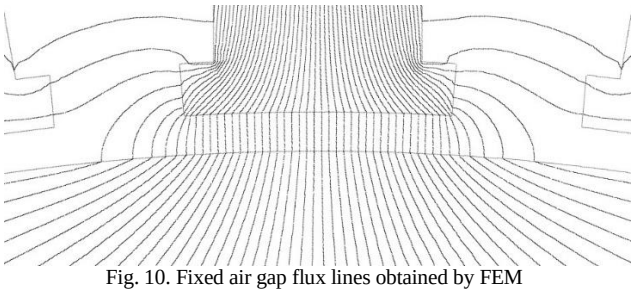

Fig. 10. Fixed air gap flux lines obtained by FEM

Figure 11. shows this decomposition and the equivalent magnetic circuit.

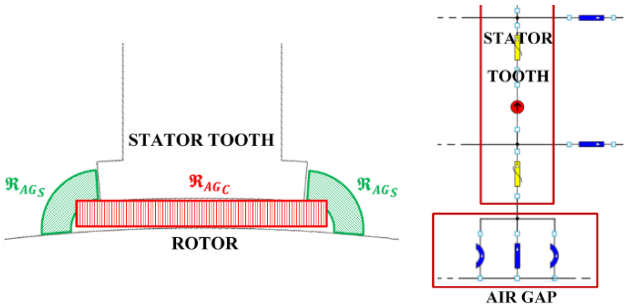

(a) (b)

Fig. 11. Identification of air gap reluctances (a) schematics of the modeled reluctances (b) equivalent magnetic circuit

As shown in figure 11(a), reluctance $\Re_{AGC}$ represents the purely radial flux path while reluctance $\Re_{AG_S}$ are curved reluctances representing the flux path crossing from the teeth opening edge to the rotor.

As explained in section C.1), $\Re_{AGC}$ is composed of a base reluctance $\Re_{AGC_{base}}$ and a complementary reluctance $\Re_{AGC_{comp}}$ such as:

$$\Re_{AGC} = \Re_{AGC_{base}} + 2 \cdot \Re_{AGC_{comp}}$$
$$\Re_{AGC_{comp}} = \frac{1}{\mu_0} \cdot \frac{AG}{L_Z \cdot (k_1 \cdot S_{OP} + k_2 \cdot AG)} \quad (3)$$

with k_1 and k_2 fitting parameters adjusted such as the model fit on the largest defined air gap and slot opening variation.

Curved reluctances displayed in figure 12 such as $\Re_{AG_S}$ are calculated using equation (4).

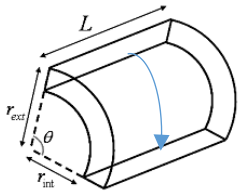

Fig. 12. 3-phase equivalent current sources by tooth

$$\Re = \frac{1}{\mu_0 \cdot \mu_r} \cdot \frac{\theta}{L \cdot \ln\left(\frac{r_{ext}}{r_{int}}\right)} \quad (4)$$

In the case of $\Re_{AG_S}$, the difficulty lies in the definition of the value of r_{ext}. The paper proposes an approximation based on geometrical considerations. In fact, the flux lines located in the exterior of the reluctance define an arc of $\frac{\pi}{2}$ such which maximal length is equal to the slot opening, giving (5):

$$r_{ext} \cdot \frac{\pi}{2} = S_{OP} \tag{5}$$

To accommodate with the case when $r_{ext} = r_{int}$, equation (6) is finally proposed:

$$r_{ext} = \max\left(\frac{2 \cdot S_{OP}}{\pi}, AG\right) \tag{6}$$

3) Generalisation to variable arigap

a) Discretization of the air gap

In the case of a variable air gap, the observation of flux lines displayed in figure 13 shows no incompatibility with a discretization process.

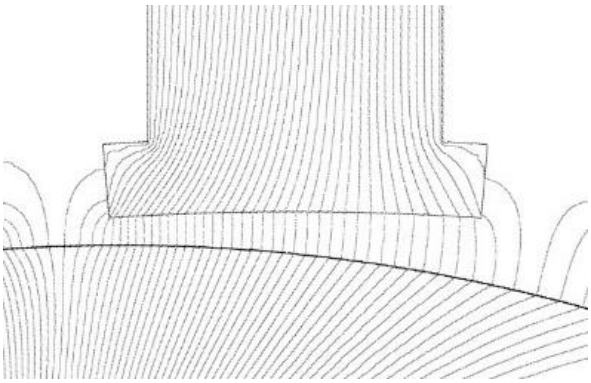

Fig. 13. Variable air gap flux lines obtained by FEM

In this way, the stator tooth pitch is split up into six parts in order to extend the validity of the model to variable air gap (see figure 14 and 15).

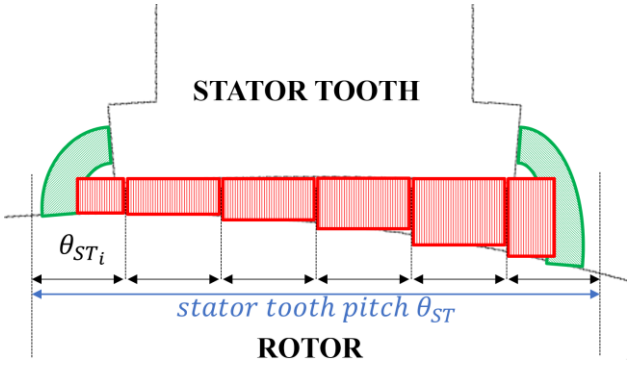

Fig. 14. Schematic of the modeled reluctances in the case of a variable air gap

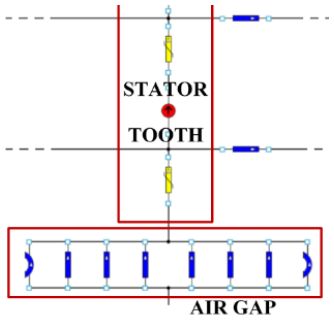

Fig. 15. Equivalent magnetic circuit in the case of a variable air gap

b) Analytical expression of the air gap as a function of the pole angle

In section C.2), all the reluctances formulas depend on the air gap value AG. With this modeling, the air gap value is varying along the rotor pole, so it is necessary to find an analytical expression of the air gap as a function of the rotor pole angle θ.

In this way, the graphical description of the geometrical parameters given by figure 16 is used.

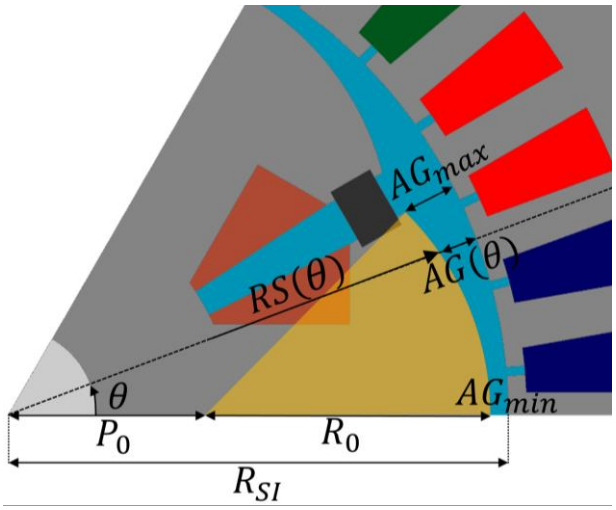

Fig. 16. Geometrical parameters describing the rotor pole

The hypothesis are the following:

- the rotor pole describe a circle of radius R_0
- the minimum value of the air gap AG_{min} is aligned with the rotor pole center

The following geometrical variables are also defined:

- P_0 is the distance between the center of the motor and the center of the circle of radius R_0
- $RS(\theta)$ is the radial distance from the center of the motor to the border of the rotor pole
- $AG(\theta)$ is the radial air gap

R_0 and P_0 are first calculated according to the values of AG_{min} and AG_{max}.

The general equation of a circle of center $A(r_a, \theta_a)$ and radius R_a in polar coordinate (r, θ) is given by (7).

$$r^2 - 2 \cdot r \cdot r_a \cdot \cos(\theta - \theta_a) + r_a^2 = R_a^2 \quad (7)$$

The application of equation (8) in the case of the rotor pole gives the value of $RS(\theta)$

$$RS(\theta) = \sqrt{P_0^2 \cdot \cos(\theta)^2 + (R_0^2 - P_0^2)} + P_0 \cdot \cos(\theta) \quad (8)$$

Then, the air gap value is simply deduced:

$$AG(\theta) = R_{SI} - RS(\theta) \quad (9)$$

c) Consideration of the rotor slot opening using a penalization function

Above the rotor slot opening, the flux path between the rotor and the stator is reduced. To consider this, a penalization function is proposed in equation (10). This function is obtained by integration of a sigmoid function.

$$cor(\theta) = k \cdot \left(\frac{\ln\left(e^{-(\lambda \cdot (\theta - \theta_{end}))}\right)}{\lambda} + (\theta - \theta_{end}) \right) \quad (10)$$

with θ_{end} the horizontal offset, k the slope coefficient and λ the curvature coefficient.

The purpose of the penalization function is to artificially increase the air gap value when approaching the slot opening (see figure 17). In this way, the air gap flux is canceled above the slot opening, reproducing the behavior of the real motor.

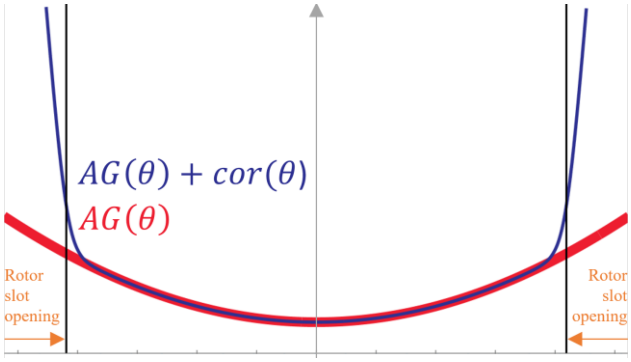

Fig. 17. Curves of the air gap value along the rotor pole angle with and without penalization function

D. Modelling of the rotor

Finally, to consider rotor behavior, multiple FEM simulation are performed with and without rotor magnet and at different stator current angle. An example of this analysis is shown in figure 18.

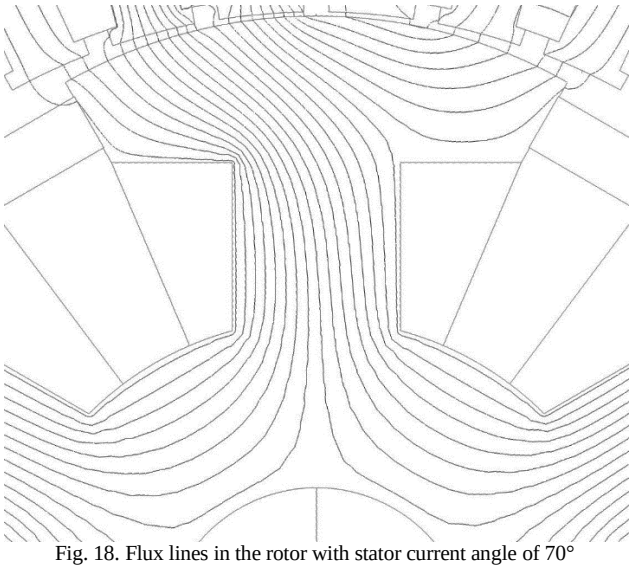

Fig. 18. Flux lines in the rotor with stator current angle of 70°

The analysis demonstrated the importance of representing radial as well as ortho-radial flux in the rotor pole head. The pole head is consequently divided in six part aligned with the six stator teeth giving the magnetic circuit displayed in figure 19.

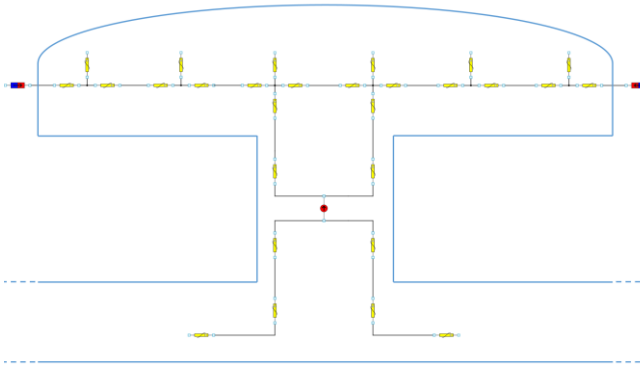

Fig. 19. Magnetic equivalent circuit of the rotor

Rotor pole head reluctances are then calculated using the expression of the pole head thickness along the rotor pole angle $PR(\theta)$, which is easily derived from the expression of $RS(\theta)$ calculated in (x).

Please note that is the case of a pure wound rotor synchronous motor (WRSM), the interpolar magnets are replaced with a rotor slot opening air reluctance. The model is thus suitable for both the design of HESM and WRSM.

At this stage, the model is fully parametrized, composed of 118 reluctances, and enables the calculation of flux in a static position. Multiple static position could be calculated by shifting the position of the rotor.

III. VALIDATION AND COMPARISON WITH THE RESULTS OBTAINED BY FINITE ELEMENTS METHOD

Results obtained with the reluctance-based model are compared and validated with a finite element model used as a reference.

1) *Results with non-linear stator, fixed air gap*

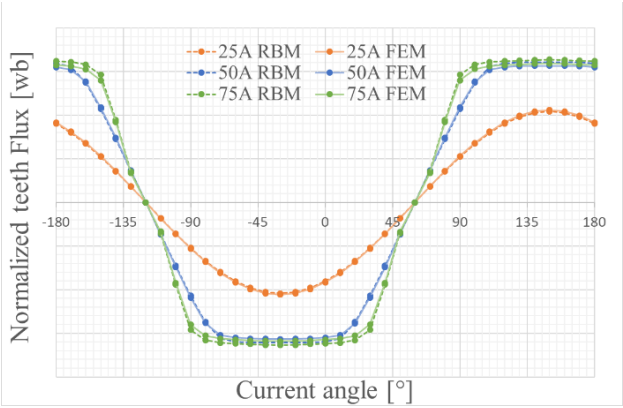

Fig. 20. FEM vs RBM flux in one tooth for different level of stator saturation as function of stator current angle;

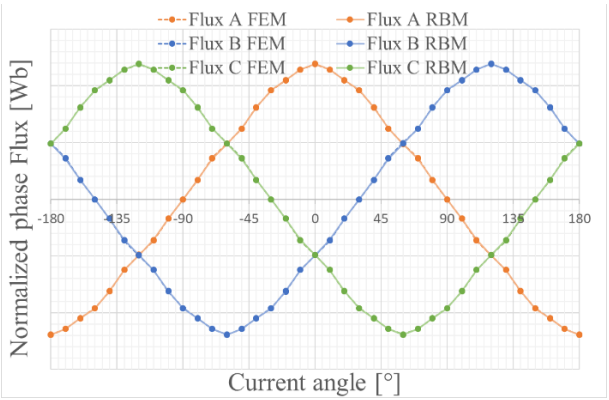

Fig. 21. FEM vs RBM phase flux as a function of stator current angle for a saturated stator and linear rotor

2) *Results with linear stator, variable air gap*

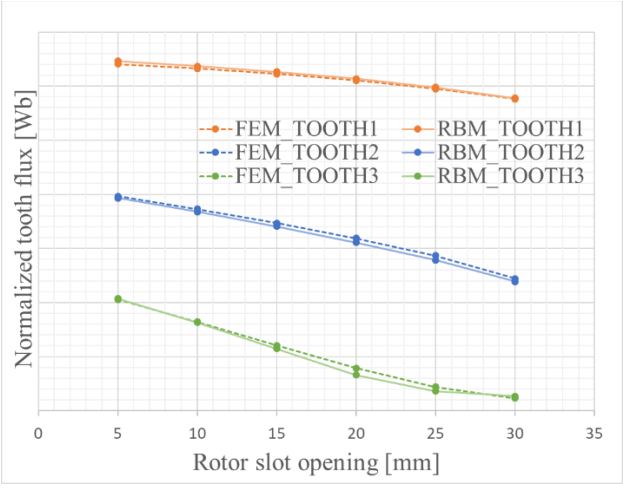

Fig. 22. FEM vs RBM teeth flux as a function of rotor slot opening with $AG_{min} = 0.5\ mm$, $AG_{max} = 2\ mm$

3) *Results with non-linear stator, variable air gap*

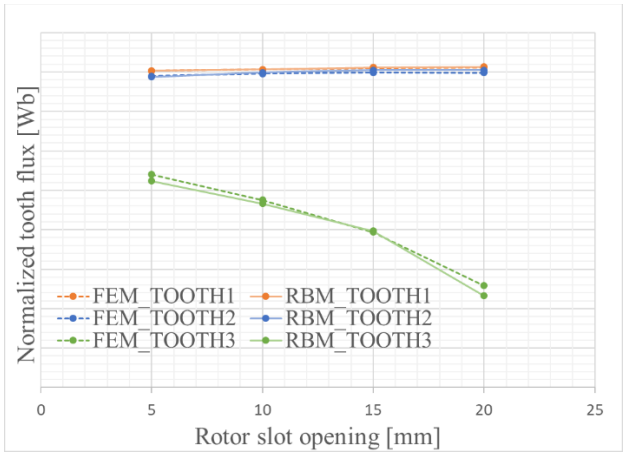

Fig. 23. FEM vs RBM teeth flux as a function of rotor slot opening with $AG_{min} = 0.5\ mm$, $AG_{max} = 1\ mm$

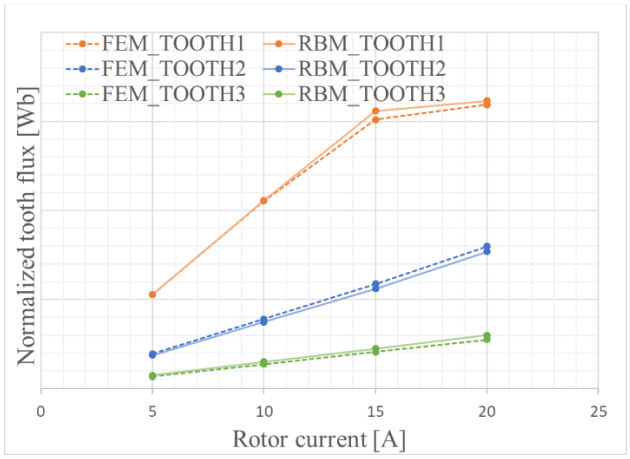

Fig. 24. FEM vs RBM teeth flux as a function of current with $AG_{min} = 0.5\ mm$, $AG_{max} = 5\ mm, R_{OP} = 10\ mm$

4) *Results with non-linear stator and rotor, variable air gap*

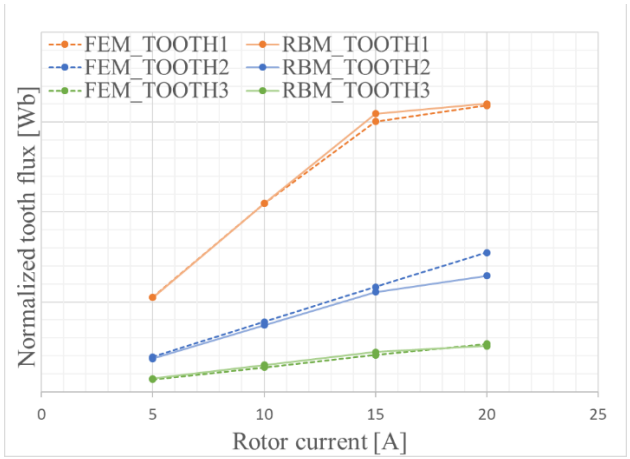

Fig. 25. FEM vs RBM teeth flux as a function of current with $AG_{min} = 0.5\ mm$, $AG_{max} = 5\ mm, R_{OP} = 10\ mm$

5) Precision, computational time and limitation of the model

This extensive comparison between RBM and FEM at each level of the modeling shows a good correlation with an error in the range of 3 to 7% depending on the saturation level and the respect of variable fitting interval.

Computation time comparison shows that RBM is 100 time faster than FEM in this case. These results are consistent with [9] conclusions on the subject.

Please note that the model can be exploited in multiple static position. It is however only suitable for the calculation of average torque.

IV. Conclusions and Future Works

In conclusion, this paper introduces a rapid and derivable model of a HESM topology derived from WRSM by adding interpolar magnets. The model is based on the calculation of equivalent reluctance circuits, allowing to deal with the parametric design of the motor. The model demonstrated a good compromise between accuracy and computation times, making it suitable for pre-design optimization tasks requiring an exploration of a large design space.

This work contributes to a broader project aiming to optimize complete drive systems and their control laws across various operating points, with future effort focusing on exploring the design for the full system, using gradient descent-based optimization algorithms.

Future works will use this modelling in an optimization process considering the complete electrical drive that contains the machine. The aim is to analyze the influence of the two-excitation modes in specific operating missions of the electrical drive, and also to obtain good performances using optimization algorithm with the electrical drive model.

References

[1] Y. Amara, L. Vido, M. Gabsi, E. Hoang, A. H. Ben Ahmed and M. Lecrivain, "Hybrid Excitation Synchronous Machines: Energy-Efficient Solution for Vehicles Propulsion," in *IEEE Transactions on Vehicular Technology*, vol. 58, no. 5, pp. 2137-2149, Jun 2009.

[2] Y. Amara, S. Hlioui, H. B. Ahmed and M. Gabsi, "Power Capability of Hybrid Excited Synchronous Motors in Variable Speed Drives Applications," in *IEEE Transactions on Magnetics*, vol. 55, no. 8, pp. 1-12, Aug. 2019, Art no. 8204312

[3] S. Hlioui *et al*., "Hybrid Excited Synchronous Machines," in *IEEE Transactions on Magnetics*, vol. 58, no. 2, pp. 1-10, Feb. 2022, Art no. 8101610

[4] A. Daanoune, A. Foggia, L. Garbuio, J. C. Mipo and L. Li, "Modeling and optimal control of a hybrid excitation synchronous machine by combining analytical and finite element models," in IEEE 2012 International Conference on Electrical Machines (ICEM), Marseille, France, 2012, pp. 2448-2453.

[5] H. Hua and Z. Q. Zhu, "Comparative Study of Series and Parallel Hybrid Excited Machines," in *IEEE Transactions on Energy Conversion*, vol. 35, no. 3, pp. 1705-1714, Sept. 2020

[6] S. Zhu, C. Liu, Y. Xu and X. Zhou, "Characteristics and experimental study on a novel Tangential/Radial Hybrid Excitation Synchronous Machine," in IEEE 2010 International Symposium on Power Electronics for Distributed Generation Systems, Hefei, China, 2010, pp. 883-886.

[7] H. C. Roters, *Electromagnetic Devices*, J. Wiley & Sons, New York, 1941.

[8] F. Wurtz, P. Kuo-Peng and E. S. De Carvalho, "The concept of Imaginary Machines for design and Setting of Optimization Problems: Application to a synchronous generator," *2012 XXth International Conference on Electrical Machines*, Marseille, France, 2012, pp. 1463-1468

[9] B. Nedjar, S. Hlioui, M. Lécrivain, Y. Amara, L. Vido and M. Gabsi, "Study of a new hybrid excitation synchronous machine," *2012 XXth International Conference on Electrical Machines*, Marseille, France, 2012, pp. 2927-2932.